Determination of the Torsion Angles of Alanine and Glycine Residues of *Bombyx Mori* Silk Fibroin and the Model Peptides in the Silk I and Silk II Forms Using 2D Spin Diffusion Solid-State NMR under Off Magic Angle Spinning

Jun Ashida,[†,‡] Kosuke Ohgo,[†] and Tetsuo Asakura*[,†]

Department of Biotechnology, Tokyo University of Agriculture and Technology, Koganei, Tokyo 184-8588, Japan, and Varian Technologies Japan Ltd., Minato, Tokyo 108-0023, Japan

Received: February 5, 2002; In Final Form: May 6, 2002

The structures of two crystalline forms of *Bombyx mori* silk fibroin, before and after the spinning process from silkworm, have been known as silk I and silk II, respectively. Most recently, we proposed a silk I structure of alternating copolypeptide $(Ala\text{-}Gly)_{15}$ as a "repeated β-turn type II structure". In this paper, two-dimensional spin diffusion solid-state NMR under off magic angle spinning was applied to determine the torsion angles of the alanine and glycine residues of the same peptide with silk II structure. The angles were determined to be ϕ, $\psi = -150°$, 150° within experimental error of ±10° for both residues, which supports an antiparallel β-sheet structure of silk II. Next, [1,2-^{13}C]glycine was incorporated into *B. mori* silk fibroin by feeding [1,2-^{13}C]glycine to silkworms to evaluate the torsion angle ψ of glycine residues in the silk fibroin directly. The angles were evaluated as $\psi = 30°$ and $\psi = 150°$ for silk I and silk II forms, respectively. The evaluation was also performed for the torsion angle of the glycine residue in $(Ala\text{-}Gly)_{15}$ in the silk I and silk II forms. The similar angles were obtained between the silk fibroin and $(Ala\text{-}Gly)_{15}$, which indicates that the structural models for the silk fibroin proposed from the structural study of $(Ala\text{-}Gly)_{15}$ are valid.

1. Introduction

The silk fibroins from silkworms can produce strong and stiff fibers at room temperature and from an aqueous solution, whereas synthetic polymeric materials with comparable properties must be processed at higher temperatures or from less benign solvents or both.[1] It is important to know the structure of the silk fibroin before spinning and after spinning to understand the mechanism of fiber formation by silkworms at the atomic level and design silk-like materials that can be produced under such mild conditions. The silk fibroin from *Bombyx mori* silkworm is a fibrous protein of which the primary structure consists mainly of a repeating sequence of six residues, $(Gly\text{-}Ala\text{-}Gly\text{-}Ala\text{-}Gly\text{-}Ser)_n$.[2] Two crystalline forms, silk I (the silk structure before spinning) and silk II (the silk structure after spinning), have been reported as the dimorphs of silk fibroin from *B. mori*. The protein exists primarily in either the silk I or random coil forms in the silk glands of the silkworm and undergoes a conformational transition to the silk II forms during the spinning process.[1]

The silk II form is characterized by an antiparallel β-sheet structure.[1,3,4] However, despite the long history of interest in the silk I form, its structure has remained poorly understood[5−15] because attempts to induce orientation of the silk I form for studies by X-ray diffraction or electron diffraction cause the silk I form to convert to the more stable silk II form. Most recently, we proposed a silk I form of alternating copolypeptide $(Ala\text{-}Gly)_{15}$ as a β-turn type II structure using 2D spin-diffusion NMR, rotational echo double resonance (REDOR) NMR, and ^{13}C chemical shift contour plots.[16] The backbone torsion angles, ϕ and ψ, of $(Ala\text{-}Gly)_{15}$ in the silk I form were determined as (−60°,130°) and (70°,30°) for alanine and glycine residues, respectively. In this model, there are both intra- and intermolecular hydrogen bonds alternatively along the backbone chain.

In general, X-ray diffraction is one of the most practical methods to obtain the detailed structure for single-crystal samples, and this method has provided the molecular structures of numerous proteins at the atomic level. However, it is necessary to prepare a single crystal of proper size for the purpose, and thus, X-ray diffraction is not suitable to determine the structure of amorphous and unoriented samples. This difficulty has excluded a large number of biologically relevant proteins and has been the impetus for the development of new techniques for determination of the structure at atomic level.

On the other hand, high-resolution liquid-state NMR became a practical method for structure determination of peptides and proteins. However, this method is not applicable to the determination of the structure of fibrous proteins in the solid state. Solid-state NMR is becoming a versatile method that can fill the vacant regions not suitable for X-ray diffraction or liquid-state NMR. The chemical shift interaction and dipolar interaction, which are mainly observed in solid-state NMR for half-spin nuclei, are used for the determination of solid-state structures.

2D spin-diffusion solid-state NMR is a powerful method to obtain the relative orientation of two chemical shift tensors of ^{13}C-labeled sites in the local molecular framework.[16−25] The spectrum represents the correlation between the resonance frequencies ω_1 before and ω_2 after a mixing time τ_m. Intra- or intermolecular spin diffusion, derived by dipolar coupling between two ^{13}C spins, occurs during τ_m. Any exchange processes that occur between different resonance frequencies will appear at off-diagonal signal intensity in the 2D spectrum.

* To whom correspondence should be addressed. E-mail address: asakura@cc.tuat.ac.jp.
† Tokyo University of Agriculture and Technology.
‡ Varian Technologies Japan Ltd.

10.1021/jp020331t CCC: $22.00
Published on Web 08/16/2002

Therefore, the relative orientation of two chemical shift tensors of the ^{13}C-labeled sites will be determined by a comparison of the experimental and simulated spectra. For several peptide compounds, the relative orientations of the chemical shift tensor and molecular frame of carbons have been reported.[26−30] Thus, when two carbonyl carbons of the neighboring residues in a peptide were ^{13}C-labeled, the torsion angles, ϕ and ψ, could be determined. If both 1-C and 2-C carbons in one residue were ^{13}C-labeled, only the torsion angle, ψ, could be determined. The same pulse sequence technique is widely used as 2D exchange NMR to study molecular dynamics. The difference between 2D exchange and 2D spin-diffusion NMR is that off-diagonal peaks in the 2D spectrum are driven by molecular reorientation or spin-diffusion.

All of the 2D spin-diffusion NMR spectra, in this work, were obtained under off magic angle spinning (OMAS) and not MAS or static. The advantages of 2D OMAS method are as follows:[19,31] (a) The mixing time could be short compared with the static condition. Sample spinning leads to the modulation of the homonuclear dipolar Hamiltonian, which depends on time. Therefore, spin diffusion was accelerated, and the τ_m could be shorten by sample spinning compared with the static condition. (b) Improvement of the signal-to-noise ratio compared with static condition could be achieved, although the ratio is much lower than that of a MAS experiment. The OMAS powder pattern spectrum is scaled by a factor of $^1/_2(3\cos^2\theta - 1)$ from the static powder pattern, where θ represents the angle between the static magnetic field, $\mathbf{B}_0$, and the sample spinning axis. Therefore, the signal intensity of the OMAS spectrum is multiplied by 1/(scaling factor) of that of static powder pattern spectrum. Moreover, overlap of powder pattern spectra of chemically nonequivalent nuclei may decrease in some cases. (c) It is easy to compare experimental and simulated spectra patterns. Under MAS condition, the spinning sideband (SSB) pattern is obtained at off-diagonal in the 2D spectrum. The SSB pattern appears discretely by every sample spinning frequency ω_r. Therefore, only intensities of the SSB pattern are used for the simulation of 2D MAS spin-diffusion spectra. On the other hand, the 2D OMAS spectrum is obtained as a powder pattern, which is widespread and similar to the static powder pattern. Therefore, both the intensity and the shape of the powder pattern spectrum are used for the simulation. It is easier to make accurate analysis with a widespread powder pattern spectrum. (d) Under the MAS condition, to obtain a phase-sensitive 2D SSB pattern, mixing time τ_m should be synchronized with a rotor period t_R as $\tau_m = nt_R$ and $t_1 + \tau_m = nt_R$, where n is an integer. Thus, well-controlled sample spinning speed is required to obtain an in-phase SSB pattern. Under the OMAS condition, well-controlled sample spinning speed is also required; however, it is not as sensitive as the MAS condition. Thus, OMAS has several advantages and can be used for the determination of torsion angles.

In this paper, the determination of the torsion angles of the alanine and glycine residues was performed with ^{13}C two-dimensional spin-diffusion solid-state NMR for $(Ala\text{-}Gly)_{15}$ in the silk II form. Then [1,2-^{13}C]glycine was incorporated into *B. mori* silk fibroin by feeding [1,2-^{13}C]glycine to silkworms to evaluate the torsion angle ψ of glycine residues in the silk fibroin directly.[8,9,29] We prepared [1,2-^{13}C]glycine-labeled natural silk fibroins in the silk I and silk II forms by incorporating [1,2-^{13}C]glycine into the silk fibroin biosynthetically.[32,33] The determination of the torsion angle, ψ, of the glycine residue in $(Ala\text{-}Gly)_{15}$ in the silk I and silk II forms was performed for a comparison.

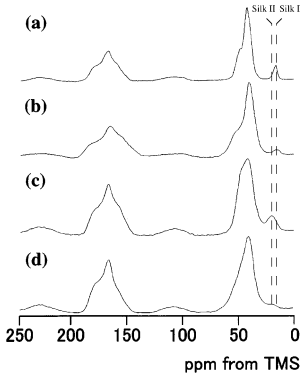

Figure 1. One-dimensional ^{13}C cross-polarization NMR spectra of *Bombyx mori* silk fibroins and $(Ala\text{-}Gly)_{15}$ samples under off magic angle spinning. The angle between the static magnetic field and sample spinning axes is fixed to be 63°. Spectrum a represents $(AG)_7$A[1,2-^{13}C]G$(AG)_7$ in the silk I form. The peptide was dissolved in 9 M LiBr and dialyzed against water. Spectrum b represents [1,2-^{13}C]glycine *B. mori* silk fibroin in the silk I form. Spectrum c represents $(AG)_7$A-[1,2-^{13}C]G$(AG)_7$ in the silk II form. The silk I peptide was dissolved in formic acid and dried. Spectrum d represents [1,2-^{13}C]glycine *B. mori* silk fibroin in the silk II form.

2. Experimental Section

Several ^{13}C selectively isotope-labeled $(Ala\text{-}Gly)_{15}$, $(AG)_5$A-[1-^{13}C]G[1-^{13}C]A$G(AG)_8$, $(AG)_6$[1-^{13}C]A[1-^{13}C]G$(AG)_8$, and $(AG)_7$A[1,2-^{13}C]G$(AG)_7$, were synthesized by the solid-phase method (Pioneer Peptide Synthesizer, Applied Biosystems Ltd.)[16] for 2D spin-diffusion experiment. To prepare the silk I sample, $(Ala\text{-}Gly)_{15}$ was dissolved in 9 M LiBr and then dialyzed against water for 4 days. For preparation of the silk II sample, the silk I sample was dissolved in formic acid and then dried at room temperature. The structures of all samples in the silk I and silk II forms were confirmed from the IR and ^{13}C CP/MAS NMR spectra.

B. mori larvae were reared in our laboratory. A total of 100 μL of 7.5−15.0% (w/v) [1,2-^{13}C]glycine (99.9 atom % ^{13}C enrichment, Mastrace, Inc. Woburn, MA) in aqueous solution was given by oral administration to 5th-instar larvae from 5-days-old to 7-days-old for 3 days: two times, morning and evening, per day for a silkworm.[29,30] To obtain silk fibroin in the silk I form, the silk glands containing [1,2-^{13}C]glycine silk fibroin were pulled out from an anesthetized 8-day-old 5th-instar larva and the gellike silk fibroin stored in the silk glands was washed in distilled water and dried. [1,2-^{13}C]Glycine silk fibroin in the silk II form was obtained from the cocoons after degumming. The ^{13}C enrichment of ^{13}C-labeled *B. mori* silk fibroin was evaluated to be about 15% from Figure 1.

The 2D spin-diffusion solid-state NMR spectra under OMAS condition were obtained using a Varian UNITY*INOVA* 400 MHz NMR spectrometer with 7 mm ϕ AutoMAS HX probe at off magic angle condition (63°) at room temperature. The sample spinning speed was 6 kHz (±3 Hz). The mixing times were set to be 2 s for both $(AG)_5$A[1-^{13}C]G[1-^{13}C]A$G(AG)_8$ and $(AG)_6$-[1-^{13}C]A[1-^{13}C]G$(AG)_8$ and 100 ms for both $(AG)_7$A[1,2-^{13}C]G-$(AG)_7$ and [1,2-^{13}C]glycine *B. mori* silk fibroins. They were optimized for spin diffusion between intramolecular specific carbons of selectively isotope-labeled alanine or glycine residues or both but no spin diffusion among intermolecular carbons. The recycle delay (2 s) was carefully determined from the 1D OMAS spectra under several recycle times for each sample. The contact time was set to 2 ms using the variable-amplitude cross polarization (VACP) technique.[34] An 81 kHz rf field strength was used for ^{1}H decoupling during evolution and acquisition periods. The number of scans of each 2D spectrum

was described in each figure caption. The angle θ between static magnetic field and sample spinning axis was determined by the measurements of scaled ^{13}C chemical shielding anisotropy (CSA) spectra of β-quinol methanol under off magic angle spinning.[31] The CSA of the benzene carbon of β-quinol methanol is 176 ppm, and both the scaling factor and the angle θ were easily calculated from the scaled CSA powder pattern under off magic angle spinning.

The principal values of the carbonyl carbon chemical shift tensors of the isotope-labeled alanine and glycine residues of the samples were determined with the spinning sideband methods under slow MAS condition with Chemagnetics Infinity 400 MHz NMR spectrometer.

3. Simulations of 2D Spin-Diffusion Solid-State NMR Spectra

The home-built calculation program was used to simulate the 2D spin-diffusion NMR spectra.[20,35] Here, a homonuclear two-spin, S_i and S_j, system is considered to simplify formalization. The total Hamiltonian is described as

$$H = H_{CS} + H_D + H_J$$

where H_{CS}, H_D, and H_J are chemical shift and Zeeman interactions, homonuclear dipolar interaction and homonuclear spin−spin coupling interaction, respectively. Each Hamiltonian is described as

$$H_{CS} = -\omega_i S_{Zi} - \omega_j S_{Zj}$$

$$H_D = \omega_D\{S_{Zi}S_{Zj} - {}^1/_4(S_{+i}S_{-j} + S_{-i}S_{+j})\}$$

$$H_J = 2\pi J\{S_{Zi}S_{Zj} + {}^1/_2(S_{+i}S_{-j} + S_{-i}S_{+j})\}$$

with

$$\omega_i = \gamma_i H_0(1 - \sigma_i)$$

$$\omega_D = h\gamma_i\gamma_j/(r_{ij}(1 - 3\cos^2\theta_{ij}))$$

where r_{ij} is the distance between the two spins, and θ_{ij} is the angle between the static magnetic field $\mathbf{B}_0$ and $\mathbf{r}_{ij}$ vectors, respectively. To simplify the above equation, new symbols are introduced as follows:[36]

$$\Sigma = \omega_i + \omega_j$$

$$\Delta = \omega_i - \omega_j$$

$$A = {}^1/_2(\omega_D + 2\pi J)$$

$$B = {}^1/_2(-\omega_D + 4\pi J)$$

Term A only perturbs the single-spin eigenvalues; however, term B is the flip-flop term of two spins and perturbs the eigenstates. We consider the product bases of the two-spin systems to evaluate the matrix components of the Hamiltonian. The total Hamiltonian is described as matrix representation

$$H = \begin{bmatrix} \Sigma + A & 0 & 0 & 0 \\ 0 & \Delta - A & B & 0 \\ 0 & B & -\Delta - A & 0 \\ 0 & 0 & 0 & -\Sigma + A \end{bmatrix}$$

In general, the time evolution of the spin systems is described by the Liouville equation of density matrix as

$$d/dt\ \rho(t) = -i[H(t),\rho(t)]$$

For static samples, the Liouville equation can be solved because $H(t)$ is independent of time. However, if $H(t)$ depends on time, such as rotating solids or anisotropic motion, it is uncommutable with itself for different times and the Liouville equation cannot be solved in overall time. Then, to diagonalize this Hamiltonian, the propagator U is introduced to solve the Liouville equation. Density matrix ρ is solved as

$$\rho(t) = U(t)\rho(0)U(t)^{-1}$$

at specific time t by using propagator $U(t)$, where $U(t)$ is

$$U(t) = T\exp\{-i\int dt'\ H(t')\}$$

where T is Dyson's time-ordering operator.[37] Therefore, the obtained free induction decay (FID) is represented as

$$S_+(t) = \mathrm{tr}\{U(t)\rho(0)U(t)^{-1}S_+(0)\}$$

and the calculated spectrum is obtained by Fourier transformation of this equation.

Generally, the propagator U should be obtained for the number of sampling points. However, this means it is necessary to diagonalize density matrix $\rho(t)$ for hundreds to thousands of times, and it would take a longer time for calculation. In our program, only sample spinning rotation for the time dependence of the Hamiltonian was considered and the dwell time (t_S) is synchronized with the rotor period (t_R) to reduce the calculation time.

$$t_R = nt_S \qquad (n = \text{integer})$$

Under this condition, the Hamiltonian is represented as

$$H(Nt_R + \Delta t) = H(\Delta t) \qquad (N = \text{integer})$$

because of the synchronization with t_R. Then propagator U is represented as

$$U(Nt_R + \Delta t) = U(\Delta t)\mathrm{U}(t_R)^N$$

Therefore, only n propagators are necessary to calculate, and the calculation time is reduced as much as possible.

The relative orientation between the chemical shift tensors of the carbonyl carbons of alanine and glycine and the molecular frame used in this work is as follows:[26−30] σ_{33} is perpendicular to the O−C′−N plane, σ_{22} is set to be parallel to the C═O bond, although σ_{22} rather deviates by about 10°,[26−30] and σ_{11} is on the O−C′−N plane and perpendicular to both σ_{22} and σ_{33}. The relative orientation between the chemical shift tensors of the methylene carbons of glycine and the molecular frame used in this work is as follows:[38] σ_{22} is along the bisector of the H−C$^\alpha$−H angle, σ_{33} is perpendicular to the H−C$^\alpha$−H plane, and σ_{11} is on the H−C$^\alpha$−H plane and perpendicular to both σ_{22} and σ_{33}. For 2D spin-diffusion NMR simulation experiments, the calculations were performed with the grid of 10° for ϕ and ψ values. An OCTANE (Silicon Graphics Inc.) workstation was used for the calculation of the theoretical spectra.

4. Results and Discussion

4.1. One-Dimensional ^{13}C Spin Diffusion NMR Spectra of (AG)$_7$A[1,2-^{13}C]G(AG)$_7$ and [1,2-^{13}C]Glycine-Labeled *B. mori* Silk Fibroins. Figure 1 shows the ^{13}C cross-polarization

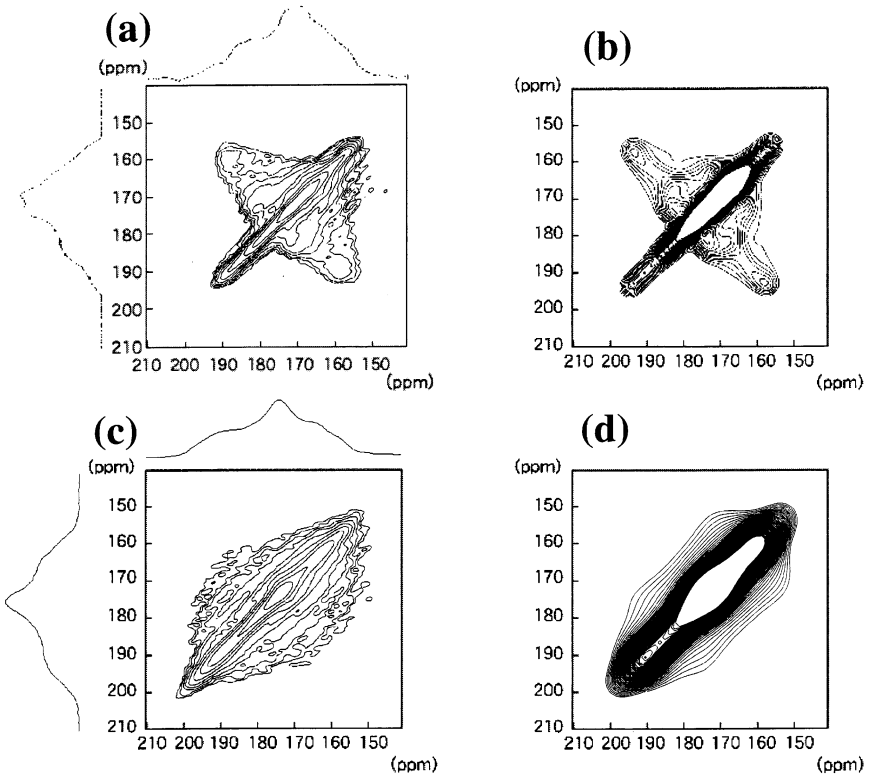

Figure 2. 2D spin-diffusion spectra of $(AG)_5A[1\text{-}^{13}C]G[1\text{-}^{13}C]AG(AG)_8$ in the (a) silk I and (c) silk II forms. The simulated spectra with the torsion angles (b) $\phi, \psi = -60°, 130°$ and (d) $\phi, \psi = -150°, 150°$ of alanine residues were also shown. The number of scans was (a) 336 and (c) 311.

off magic angle spinning NMR spectra of model peptide $(AG)_7A[1,2\text{-}^{13}C]G(AG)_7$ and [1,2-^{13}C]glycine-labeled *B. mori* silk fibroin. Spectra a and b are those of the model peptide and *B. mori* silk fibroin in the silk I forms, respectively. Similarly, spectra c and d are those of the model peptide and *B. mori* silk fibroin in the silk II forms, respectively. The main high-field peaks at approximately 40 ppm in spectra a and b can be assigned to the glycine $^{13}C^{\alpha}$ carbon coupled with glycine ^{13}CO carbons, which was incorporated into these samples, because of the very small intensity of natural abundance alanine C^{β} peak at 16.6 ppm. Thus, it is clear that [1,2-^{13}C]glycine could be incorporated into silk fibroin without cleavage of the ^{13}C double-labeled bond. The alanine C^{β} chemical shift is conformation-dependent, and the chemical shift value of 16.6 ppm clearly shows that these two samples take the silk I form.[14−16] On the other hand, judging from the alanine C^{β} chemical shift (20 ppm) in spectra c and d, it is clear that the corresponding samples take antiparallel β-sheet structure.[14,15]

4.2. 2D Spin-Diffusion Solid-State NMR Spectra of $(AG)_5A[1\text{-}^{13}C]G[1\text{-}^{13}C]AG(AG)_8$ in the Silk I and Silk II Forms. The 2D spin-diffusion solid-state NMR spectra (only the carbonyl carbon regions were expanded) of $(AG)_5A[1\text{-}^{13}C]G[1\text{-}^{13}C]AG(AG)_8$ in the silk I (panel a) and silk II (panel c) forms are shown in Figure 2 together with the simulated spectra of the torsion angles $\phi, \psi = -60°, 130°$ (panel b) and $\phi, \psi = -150°, 150°$ (panel d) of alanine residues. The observed spectrum (panel a) of $(AG)_5A[1\text{-}^{13}C]G[1\text{-}^{13}C]AG(AG)_8$ in the silk I form was essentially the same as that reported for$(AG)_6A[1\text{-}^{13}C]G[1\text{-}^{13}C]AG(AG)_7$ in the silk I form previously.[16] Thus, the observed spectral pattern is independent of the position of the alanine residue in the model peptide except for the end position. The good agreement between the observed (panel a) and simulated (panel b) spectra supports the silk I structure proposed previously.[16] On the other hand, the observed silk II spectrum (panel c) is quite different from the silk I spectrum (panel a). Namely, the observed spectrum displays a pronounced intensity along the diagonal element, which is reasonable for a β-sheet structure because the carbonyl tensors are aligned parallel to one another. The 2D spin-diffusion solid-state NMR spectra were calculated as a function of torsion angles ϕ and ψ of the alanine residues of $(Ala\text{-}Gly)_{15}$ for each 10° for all possible values $-180° < \phi, \psi < 180°$. The torsion angles of (−150°, 150°) for alanine residues were determined as shown in Figure 2d. The experimental error of the angle was ±10°.

4.3. 2D Spin-Diffusion Solid-State NMR Spectra of $(AG)_6[1\text{-}^{13}C]A[1\text{-}^{13}C]G(AG)_8$ in the Silk I and Silk II Forms. The 2D spin-diffusion solid-state NMR spectra (only the carbonyl carbons region was expanded) of $(AG)_6[1\text{-}^{13}C]A[1\text{-}^{13}C]G(AG)_8$ in the silk I (panel a) and silk II (panel c) forms are shown in Figure 3, together with the simulated spectra of the torsion angles $\phi, \psi = 70°, 30°$ (panel b) and $\phi, \psi = -150°, 150°$ (panel d) of glycine residues. The agreement between the observed (panel a) and calculated spectra (panel b) for the silk I form was extremely good.

On the other hand, the observed silk II spectrum (panel c) is quite different from the silk I spectrum (panel a). The 2D spin-diffusion solid-state NMR spectra were calculated as a function of ϕ and ψ of the glycine residues of $(Ala\text{-}Gly)_{15}$ for each 10° for all possible values $-180° < \phi, \psi < 180°$, previously.[16] The torsion angles of (−150°, 150°) for glycine residues were determined as shown in Figure 3d. The experimental error of the angle is also ±10°. Thus, both alanine and glycine residues of $(Ala\text{-}Gly)_{15}$ take antiparallel β-sheet structure with the torsion angles of $\phi = -150°, \psi = 150°$. However, it is difficult to obtain the torsion angles of both residues using this method for the silk fibroin because the ^{13}C labeling of specific two carbonyl carbons of silk fibroins is difficult. Thus in the next section, we will try to use [1,2-^{13}C]glycine-labeled silk fibroin.

4.4. 2D Spin-Diffusion Solid-State NMR Spectra of $(AG)_7A[1,2\text{-}^{13}C]G(AG)_7$ and [1,2-^{13}C]Glycine-Labeled *B. mori* Silk Fibroins in the Silk I and Silk II Forms. The 2D spin-diffusion

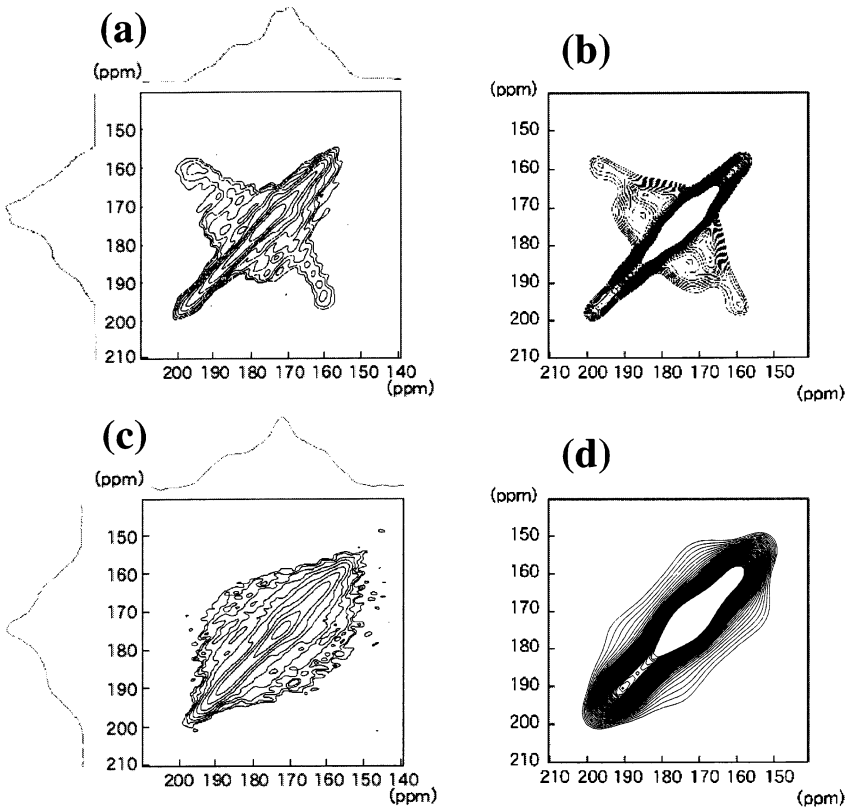

Figure 3. 2D spin-diffusion spectra of $(AG)_7$[1-^{13}C]A[1-^{13}C]G $(AG)_7$ in the (a) silk I and (c) silk II forms. The simulated spectra with the torsion angles (b) ϕ, ψ = 70°, 30° and (d) ϕ, ψ = −150°, 150° of glycine residues were also shown. The number of scans was (a) 428 and (c) 88.

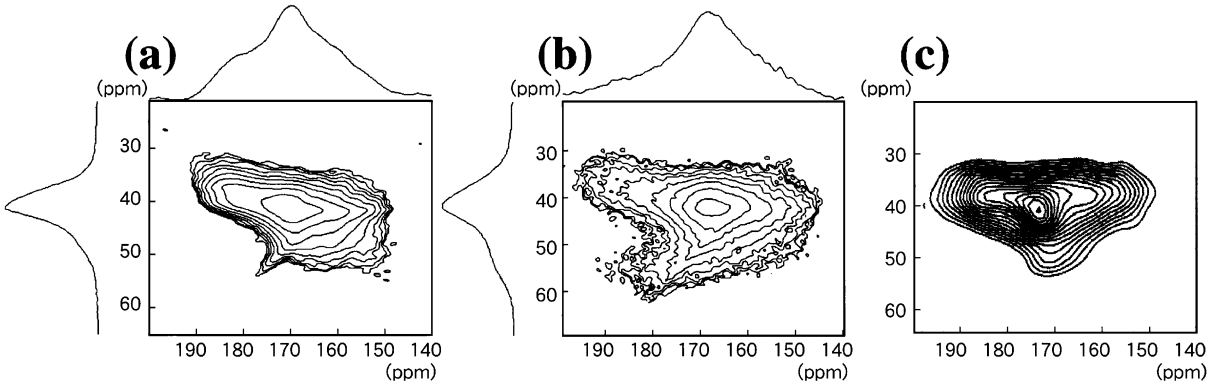

Figure 4. 2D spin-diffusion spectra of (a) $(AG)_7$A[1,2-^{13}C]G$(AG)_7$ and (b) [1,2-^{13}C]glycine *B. mori* silk fibroin in the silk I forms. The number of scans was (a) 812 and (b) 304. The simulated spectrum of glycine residue with the torsion angle ψ = 30° (panel c) was also shown.

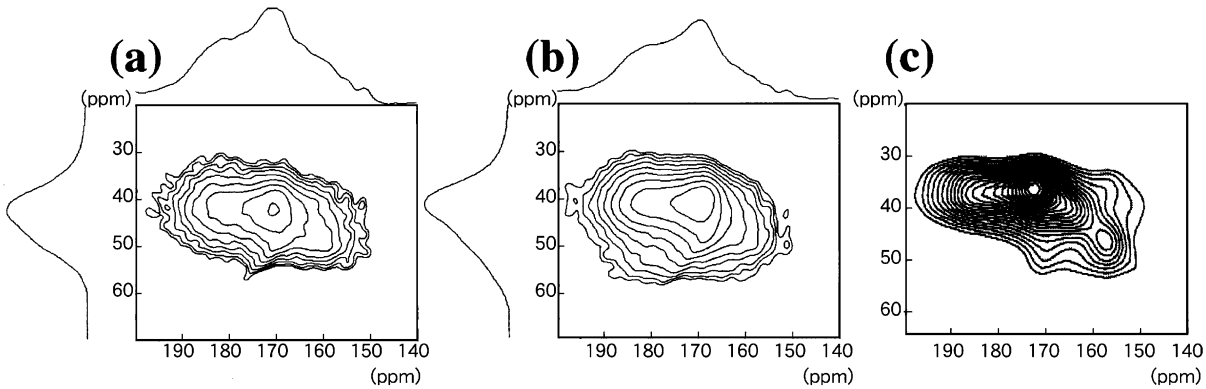

Figure 5. 2D spin-diffusion spectra of (a) $(AG)_7$A[1,2-^{13}C]G$(AG)_7$ and (b) [1,2-^{13}C]glycine *B. mori* silk fibroin in the silk II forms. The number of scans was (a) 585 and (b) 1000. The simulated spectrum of glycine residue with the torsion angle ψ = 150° (panel c) was also shown.

solid-state NMR spectra (only one of the cross-peaks of carbonyl carbon and methylene carbon were expanded) of (a) $(AG)_7$A-[1,2-^{13}C]G$(AG)_7$ and (b) [1,2-^{13}C]glycine *B. mori* silk fibroin in the silk I form are shown in Figure 4, together with the

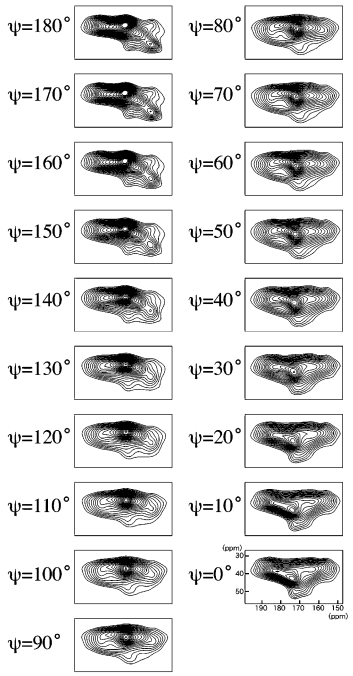

Figure 6. The 2D spin-diffusion solid-state NMR spectra calculated as a function of torsion angle ψ of glycine residue for each 10° in the range of 0° to 180°.

simulated spectrum (panel c) with the torsion angle $\psi = 30°$ of glycine residues. Also, the 2D spin-diffusion solid-state NMR spectra of (a) $(AG)_7A[1,2\text{-}^{13}C]G(AG)_7$ and (b) [1,2-^{13}C]glycine *B. mori* silk fibroin in the silk II form are shown in Figure 5, together with the simulated spectrum of the torsion angle $\psi = 150°$ of glycine residues. The calculated 2D spin-diffusion solid-state NMR spectra as a function of ψ of the glycine residues are shown in Figure 6. The difference in the spectrum is small because the CSA of the methylene carbon of the glycine residue is not so large. The CSA of carbonyl carbons is approximately 160 ppm, and the observed CSA is about 32 ppm when the scaling factor = 0.2 or −0.2, but the CSA of methylene carbons is approximately 40 ppm, and the observed CSA is only about 8 ppm at same scaling factor. Therefore, it was difficult to determine the exact torsion angle ψ from the simulated spectra. However, by comparing these spectra carefully, there is obvious difference between $\psi > 90°$ and $\psi < 90°$ regions. In all spectra, a ridge from σ_{33} to σ_{11} via σ_{22} of the carbonyl carbon could be seen in the 2D powder pattern spectra. However, at the region of $\psi > 90°$, the ridge from σ_{33} to σ_{22} of carbonyl carbon is almost parallel to the F_2 axis, and the angle between the ridge from σ_{33} to σ_{22} and the ridge from σ_{22} to σ_{11} of the carbonyl carbon becomes larger as an increment of ψ. On the other hand, at the region of $\psi < 90°$, the straight ridge from σ_{33} to σ_{11} of carbonyl carbon which is almost parallel to the F_2 axis, and also the ridge from σ_{33} to σ_{22} of carbonyl carbon could be seen. For glycine residues, the tentative values of ψ is 150° and 30° for β-sheet and β-turn structure, respectively.[39] Therefore, it is easy to distinguish the structure between β-sheet and β-turn from the cross-peak of carbonyl and methylene carbons in the 2D spin-diffusion solid-state NMR spectrum.

5. Conclusions

By using two-dimensional spin-diffusion solid-state NMR under off magic angle spinning and [1,2-^{13}C]glycine silk fibroin, we could determine the atomic level structure of *Bombyx mori* silk fibroin. Namely, the torsion angle ψ of glycine residue in the natural silk fibroin was determined directly as $\psi = 30°$ and $\psi = 150°$ for the silk I and silk II forms, respectively. The torsion angles of the glycine residue in the model peptide, $(Ala\text{-}Gly)_{15}$, were also determined as $\psi = 30°$ and $\psi = 150°$ for the silk I and silk II forms, respectively. This indicates that the model peptide is also applicable as the structural model for the silk fibroin. The backbone torsion angles ϕ and ψ of $(Ala\text{-}Gly)_{15}$ in the silk I structure have been determined as −60°, 130° and 70°, 30° for alanine and glycine residues, respectively.[16] For $(Ala\text{-}Gly)_{15}$ in the silk II structure, the torsion angles were determined to be ϕ, $\psi = -150°$, 150° for both alanine and glycine residues in this paper. The experimental error was ±10°.

Acknowledgment. T.A. acknowledges supports from Bio-oriented Technology Research Advancement Institution.

References and Notes

(1) Asakura, T., Kaplan, D. L. In *Encyclopedia of Agriculture Science*; Arutzen, C. J., Ed.; Academic Press: New York, 1994.
(2) Fraser, B.; MacRae, T. P. *Conformations of Fibrous Proteins and Related Synthetic Polylpeptides*; Academic Press: New York, 1973.
(3) Marsh, R. E.; Corey, R. B.; Pauling, L. *Biochim. Biophys. Acta* **1955**, *16*, 1.
(4) Takahashi, Y.; Gehoh, M.; Yuzuhira, K. *Int. J. Biol. Macromol.* **1999**, *24*, 127.
(5) Konishi, T.; Kurokawa, M. *Sen'i Gakkaishi* **1968**, *24*, 550.
(6) Lotz, B.; Keith, H. D. *J. Mol. Biol.* **1971**, *61*, 201.
(7) Lotz, B.; Cesari, F. D. *Biochimie* **1979**, *61*, 205.
(8) Saito, H.; Tabeta, R.; Asakura, T.; Iwanaga, Y.; Shoji, A.; Ozaki, T.; Ando, I. *Macromolecules* **1984**, *17*, 1405.
(9) Asakura, T.; Kuzuhara, A.; Tabeta, R.; Saito, H. *Macromolecules* **1985**, *18*, 1841.
(10) Asakura, T.; Yamaguchi, T. *J. Seric. Sci. Jpn* **1987**, *56*, 300.
(11) Anderson, J. P. *Biopolymers* **1998**, *45*, 307.
(12) Okuyama, K.; Takahashi, K.; Nakajima, Y.; Hasegawa, Y.; Hirabayashi, K.; Nishi, N. *J. Seric. Sci. Jpn* **1988**, *57*, 23.
(13) Fossey, S. A.; Nemethy, G.; Gibson, K. D.; Scheraga, H. A. *Biopolymers* **1991**, *31*, 1529.
(14) Asakura, T.; Demura, M.; Date, T.; Miyashita, M.; Ogawa, K.; Williamson, M. P. *Biopolymers* **1997**, *41*, 193.
(15) Asakura, T.; Iwadate, M.; Demura, M.; Williamson, M. P. *Int. J. Biol. Macromol.* **1999**, *24*, 167.
(16) Asakura, T.; Ashida, J.; Yamane, T.; Kameda, T.; Nakazawa, Y.; Ohgo, K.; Komatsu, K. *J. Mol. Biol.* **2001**, *306*, 291.
(17) Edzes, H. T.; Bernards, J. P. C. *J. Am. Chem. Soc.* **1984**, *106*, 1515.
(18) Henrichs, P. M.; Linder, M. *J. Magn. Reson.* **1984**, *58*, 458.
(19) Hagemeier, A.; Schmidt-Rohr, K.; Spiess, H. W. *Adv. Magn. Reson.* **1989**, *13*, 85.
(20) Ashida, J.; Kuwahara, D.; Uegaki, T.; Terao, T. *Proc. NMR Conf., Kyoto* **1990**, 245−246.
(21) Luz, Z.; Spiess, H. W.; Titman, J. J. *Isr. J. Chem.* **1992**, *32*, 145.
(22) Dabbagh, G.; Weliky, D. P.; Tycko, R. *Macromolecules* **1994**, *27*, 6183.
(23) Kuemmerlen, J.; van Beek, J. D.; Vollrath, F.; Meier, B. H. *Macromolecules* **1996**, *29*, 2920.
(24) Weliky, D. P.; Tycko, R. *J. Am. Chem. Soc.* **1996**, *118*, 8487.
(25) Tycko, R.; Weliky, D. P.; Berger, A. E. *J. Chem. Phys.* **1996**, *105*, 7915.
(26) Oas, T. G.; Hartzell, C. J.; Dahlquist, F. W.; Drobny, G. P. *J. Am. Chem. Soc.* **1987**, *109*, 5962.
(27) Hartzell, C. J.; Whitfield, M.; Oas, T. G.; Drobny, G. P. *J. Am. Chem. Soc.* **1987**, *109*, 5966.
(28) Teng, Q.; Cross, T. A. *J. Magn. Reson.* **1989**, *85*, 439.
(29) Demura, M.; Minami, M.; Asakura, T.; Cross, T. A. *J. Am. Chem. Soc.* **1998**, *120*, 1300.
(30) Asakura, T.; Yamazaki, Y.; Koo, W. S.; Demura, M. *J. Mol. Struct.* **1998**, *446*, 179.
(31) Nakai, T.; Ashida, J.; Terao, T. *J. Chem. Phys.* **1988**, *88*, 6049.
(32) Schmidt-Rohr, K. *J. Am. Chem. Soc.* **1996**, *118*, 7601.
(33) Schmidt-Rohr, K. *Macromolecules* **1996**, *29*, 3975.
(34) Peersen, O.; Wu, X.; Kustanovich, I.; Smith, S. O. *J. Magn. Reson. Ser. A* **1993**, *104*, 334.
(35) Levitt, M. H.; Raleigh, D. P.; Creuzet, F.; Griffin, R. G. *J. Chem. Phys.* **1990**, *92*, 6347
(36) Nakai, T. Private communication.
(37) Mehring, M. *Principles of High-Resolution NMR in Solids*; Springer-Verlag: Berlin, 1983.
(38) Haberkorn, R. A.; Stark, R. E.; van Willigen, H.; Griffin, R. G. *J. Am. Chem. Soc.* **1981**, *103*, 2534.
(39) Chou, P. Y.; Fasman, G. D. *J. Mol. Biol.* **1977**, *115*, 135.